BBA - Molecular Basis of Disease 1865 (2019) 2138–2148

Contents lists available at ScienceDirect

BBA - Molecular Basis of Disease

journal homepage: www.elsevier.com/locate/bbadis

# METTL14 is essential for β-cell survival and insulin secretion

Jun Liu[b,1], Guanzheng Luo[c,1], Juan Sun[a], Lili Men[d], Honggang Ye[a], Chuan He[b], Decheng Ren[a,*,2]

[a] Department of Medicine, University of Chicago, Chicago, IL 60637, USA
[b] Department of Chemistry, University of Chicago, Chicago, IL 60637, USA
[c] School of Life Science, Sun Yat-sen University, Guangzhou 510275, China
[d] Department of Endocrinology, First Affiliated Hospital of Dalian Medical University, Dalian 116011, China

ARTICLE INFO

*Keywords:*
METTL14
m$^6$A
β-Cells
Insulin secretion

ABSTRACT

Defects in the development, maintenance or expansion of β-cell mass can result in impaired glucose metabolism and diabetes. $N^6$-methyladenosine affects mRNA stability and translation efficiency, and impacts cell differentiation and stress response. To determine if there is a role for m$^6$A in β-cells, we investigated the effect of *Mettl14*, a key component of the m$^6$A methyltransferase complex, on β-cell survival and function using rat insulin-2 promoter-Cre-mediated deletion of *Mettl14* mouse line (βKO). We found that *βKO* mice with normal chow exhibited glucose intolerance, lower levels of glucose-stimulated insulin secretion, increased β-cell death and decreased β-cell mass. In addition, HFD-fed *βKO* mice developed glucose intolerance, decreased β-cell mass and proliferation, exhibited lower body weight, increased adipose tissue mass, and enhanced insulin sensitivity due to enhanced AKT signaling and decreased gluconeogenesis in the liver. HFD-fed *βKO* mice also showed a decrease in *de novo* lipogenesis, and an increase in lipolysis in the liver. RNA sequencing in islets revealed that Mettl14 deficiency in β-cells altered mRNA expression levels of some genes related to cell death and inflammation. Together, we showed that Mettl14 in β-cells plays a key role in β-cell survival, insulin secretion and glucose homeostasis.

## 1. Introduction

β-Cell mass is determined by the balance between β-cell differentiation, proliferation, neogenesis and death. The process of β-cell differentiation occurred during embryogenesis is a complicated signaling cascade which requires dynamic changes of transcription factor expression levels that need to occur in appropriate sequence and within appropriate timelines [1]. β-Cell proliferation proceeds at a high rate during late embryogenesis but begins to decline postnatally [2,3], and keeps at a low rate which may gradually decline with age during adulthood [4,5]. The β-cell death, primarily through apoptosis, occurs at very low rate during embryogenesis, but may have a transient burst at weaning, which may be associated with islet remodeling or changes in β-cell maturation [3]. As for β-cell neogenesis, it is still in debate regarding whether or to what extent it occurs in the postnatal and adult stages under normal circumstances [6,7]. Under normal circumstances during adulthood, the population of β-cells is maintained with steady low levels of proliferation and apoptosis. The maintenance of β-cell mass during adulthood is important to maintain glucose homeostasis and prevent diabetes [8]. Defects in development, maintenance, or expansion of β-cells can result in impaired glucose metabolism and diabetes. Both insulin biosynthesis and secretion are dynamically regulated in β-cells in response to altered metabolic demand. Pancreatic β-cells metabolically regulate physiology of glucose homeostasis primarily through the secretion of insulin. Plasma glucose concentration is the primary regulator of insulin secretion from β-cells [9]. Amino acids, fatty acids, incretins, some neurotransmitters and pituitary hormones can also affect insulin secretion [10].

$N^6$-methyl-adenosine (m$^6$A) is the most prevalent modification in eukaryotic mRNA [11]. In mammals, m$^6$A occurs on average at ≥3 sites per mRNA molecule, and tens of thousands of m$^6$A sites exist in the mRNA transcriptome [12]. m$^6$A methylated transcripts are recognized by reader proteins that regulate RNA splicing, export, translation and degradation [13,14]. This modification is reversible and monitored by "writer" and "eraser" proteins. A writer complex including METTL3 (methyltransferase-like 3), METTL14 (methyltransferase-like 14), WTAP (Wilm's-tumor-1-associated protein) along with other regulatory subunits, catalyzes the m$^6$A methylation of mRNA. At least two eraser

* Corresponding author at: Department of Medicine, The University of Chicago, 5841 S. Maryland Avenue, MC 1027, Chicago, IL 60637, USA.
*E-mail address:* ren_decheng@lilly.com (D. Ren).
[1] These authors contributed equally.
[2] Present address: Eli Lilly and Company, 893 Delaware St, Indianapolis, IN 46225, USA.

https://doi.org/10.1016/j.bbadis.2019.04.011
Received 23 February 2018; Received in revised form 20 December 2018; Accepted 6 January 2019
Available online 26 April 2019
0925-4439/ 

proteins, FTO (obesity-associated protein) and ALKBH5 (AlkB Family Member 5), help reverse this modification. $m^6A$ in mRNA modification is essential for mammals, and abnormal $m^6A$ methylation could result in dysfunction of mRNA and lead to disease [13]. $m^6A$ modifications have been implicated in embryonic stem cell maintenance and differentiation, circadian rhythm, heat shock response, meiotic progression, and neuronal function [15–19]. However, how $m^6A$ methylation affects β-cell homeostasis and the underlying mechanism remains not fully elucidated. The studies have shown that knockdown of METTL14 significantly decreases $m^6A$ levels on mRNAs [20]. In this study, we used β-cell specific Mettl14 knockout mice to test the hypothesis that METTL14 plays an important role in β-cell homeostasis.

## 2. Materials and methods

### 2.1. MIN6 cell culture

Mouse MIN6 insulinoma cells were cultured in Dulbecco's modified Eagle's medium supplemented with 15% FBS, antibiotics (100 units/mL penicillin and 100 μg/mL streptomycin), 1 mM sodium pyruvate, 10 mM HEPES, and 50 μM β-mercaptoethanol. The cells were maintained at 37 °C in an atmosphere of 5% $CO_2$ and 100% humidity.

### 2.2. Quantification of mRNA levels and lentivirus-mediated shRNA expression

pLKO.1-Mettl14 shRNA lentivirus was prepared as previously described [21]. Lentivirus was added to the medium on day 1. TaqMan assay numbers were: Hmbs, Mm00660262; Mouse ACTB, 4352933; Pdx1, Mm00435565; METTL14, Mm01318173. The other primers used in real-time RT-PCR experiments were listed below: Tnfrsf1a, forward-TGCGAGGTGTGTGATAAAGG, reverse-GGAAATGCGTCTCACTCAGG; Tnfrsf11b forward-CCACAATGAACAAGTGGCTG, reverse-GCAAGTAC TTTGGAGGAAGGG; C9 forward-TCGCAAACCTTGGAATGTAGT, reverse-CTCGGTTGATGGCTTTGAAT; FgL2 forward-GAACACATGCAGT CACAGCC, reverse-AGGGGTAACTCTGTAGGCCC; Gas2 forward-GTCG ATACCGAGTGGGAGAG, reverse-CAGATAGCCAGCGAAGGTCT; PLg forward-CCAGAGAACTTCCCAGATGC, reverse-AGTATTCCCACCTGAC GCTC; Orm1 forward-TTCCAGAAGGCTGTCACACA, reverse-AGCTGCT TCTTCTCCTGCTG; Ptger3 forward-TGGATCCCTGGGTTTATCTG, reverse-GGGAAACAGGTACTGCAATGA; Saa2 GTCTTCTGCTCCCTGCT CCT, reverse-TCATGTCAGTGTAGGCTCGC; C3 forward-GGCCTTCTCT CTAACAGCCA, reverse-TGCAGGTGACTTTGCTTTTG; Saa1 forward-GTCTTCTGCTCCCTGCTCC, reverse-TCATGTCAGTGTAGGCTCGC; F2 forward-CCCGGATTCGAATTACTGAC, reverse-CCTCCACTGTCACCTT CACA; Trf forward-GCTTTCAGGTGTCTCGTTGA, reverse-CAGATTCTT AGCCCATTCGG; DapL1 forward-GCAGTGAAAGCTGGAGGGATGCG, reverse-TGTGCCGTGTGAACTGTCGCTG; Reg1 forward-ACTGGACTCC ATGATCCCAA, reverse-TGTTAGGAGACCCAGTTGCC; Reg2 forward-GCTTCCAATGTCTGGACTGG, reverse-GTGGCCCATGACTTGAAGAG. The blots were probed with antibodies against α-Tubulin (T6199, Sigma), Actin (A-3853; Sigma), Proinsulin (8138, cell signaling), METTL14 (HPA038002, sigma). Antibody detection was accomplished using enhanced chemiluminescence (PerkinElmer) and LAS-3000 Imaging system (FUJIFILM).

### 2.3. Quantitation of cell death

Cell death was quantified by *propidium iodide* (PI) staining followed by flow cytometric analyses (FACS) using a FACS Caliber (BD Bioscience) and FlowJo software [22]. 20 μM Z-VAD-FMK (carbobenzoxy-valyl-alanyl-aspartyl-[Omethyl]-fluoromethylketone) was added to the medium 2 h prior to treatment of MIN6 cells by METTL14 shRNA lentivirus. Z-VAD was added to the cells on day 1 and day 3.

### 2.4. TUNEL staining

The apoptotic cell death was determined by the terminal deoxynucleotidyltransferase-mediated dUTP nick end labeling (TUNEL) labeling (Promega) according to the manufacturer's instructions.

### 2.5. Immunohistochemistry

The tissues were fixed with 4% formaldehyde. Prior to immunostaining, slices underwent an epitope retrieval protocol where slices were treated for 30 min with a buffer containing 10 mM sodium citrate, pH 9 in Tris buffer saline (TBS). Slices were then, blocked in TBS containing 5% normal donkey serum and 0.3% Triton X-100 for 1 h at room temperature, sections were transferred to primary antibody containing 0.3% Triton X-100 with 1% BSA and incubated at 4 °C for 48 h. Antibodies used included: insulin (1:200, Dako) and glucagon (1:100, Sigma). Secondary antibodies were diluted in 4% normal serum at 1:500 for 1 h at room temperature.

### 2.6. RNA isolation

Total RNA was isolated with TRIZOL reagent (Invitrogen). mRNA was extracted from the total RNA using the Dynabeads® mRNA Purification Kit (Invitrogen), followed by removal of contaminating rRNA with the RiboMinus transcriptome isolation kit (Invitrogen). mRNA concentration was measured by UV absorbance at 260 nm.

### 2.7. LC-MS/MS quantification of $m^6A$ in poly(A)-mRNA

100–200 ng of mRNA was digested by nuclease P1 (1 U) in 25 μL of buffer containing 20 mM of NH4Ac at 42 °C for 2 h, followed by the addition of NH4HCO3 (1 M, 3 μL) and alkaline phosphatase (0.5 U) and incubation at 37 °C for 2 h. The sample was then filtered (0.22 μm pore size, 4 mm diameter, Millipore), and 5 μL of the solution was injected into the LC-MS/MS. The nucleosides were separated by reverse phase ultra-performance liquid chromatography on a C18 column with online mass spectrometry detection using Agilent 6410 QQQ triple-quadrupole LC mass spectrometer in positive electrospray ionization mode. The nucleosides were quantified by using the nucleoside to base ion mass transitions of 282 to 150 ($m^6A$), and 268 to 136 (A). Quantification was performed by comparison with a standard curve obtained from pure nucleoside standards run with the same batch of samples. The ratio of $m^6A$ to A was calculated based on the calibrated concentrations.

### 2.8. mRNA-seq

Total RNA was isolated from mouse samples. Polyadenylated RNA was further enriched from total RNA by using Dynabeads® mRNA Purification Kit (Invitrogen). RNA library preparation followed the protocol of Illumina Truseq Stranded mRNA Library Prep Kit. Sequencing was performed at the University of Chicago Genomics Facility on an Illumina HiSeq2500 machine in single-read mode with 50 bp per read.

### 2.9. $m^6A$-seq and gene expression analysis

Total RNA was extracted from MIN6 cells. After mRNA purification and fragment, $m^6A$-specific antibodies (Synaptic Systems) are used to immunoprecipitate RNA. RNA is reverse-transcribed to cDNA and sequenced. Deep sequencing provides high-resolution reads of $m^6A$-methylated RNA [23]. Sequencing reads were aligned to mouse genome (mm9) by Tophat with Bowtie1 incorporated. Only unique mapping reads were retained for the following analysis. The exomePeak software package was introduced to identify $m^6A$ peaks. Briefly, reads from immunoprecipitated samples were compared to reads from input samples. The enriched region were identified and concatenated as

candidate m$^6$A peak. FDR < 0.05 was set to filter the low-confidence peaks. Peaks were then annotated to transcriptome based on UCSC Refseq database. The RNA-seq data from input samples were reused to compute the differentially expressed gene between METTL14 KD and control MIN6 cells. Cufflinks software package was used to calculate the fpkm value for each gene representing the relative expression level. Q-value < 0.05 was set as the cutoff to select the significant DE genes. Up-regulated and down-regulated genes were separated to do GO analysis by using DAVID tool.

### 2.10. Isolation primary mouse pancreatic islets

Mouse islets were isolated by using collagenase and filtration as previously described [24].

### 2.11. Generation of floxed Mettl14 mice

We genetically engineered mice harboring a conditionally removable allele of METTL14 on chromosome 3. Using a traditional recombineering approach, we generated a targeting construct with a single loxP site in intron 6 and a FRT-flanked neomycin resistance gene coupled with a loxP site in intron 9. These exons were targeted, because they contain the DPWW active motif. We transfected the targeting construct into 129 mouse ES cells, selected for neomycin resistance, screened for homologous recombination by Southern blotting, and used selected clones to generate chimeric mice by injection into Black-6 (Bl6) mouse blastocysts. Chimeric mice were bred to wild type Bl6 mice to test for germline transmission of the mutant allele, which was identified by PCR. The PCR-positive lines were crossed with commercially available mice containing either a b-actin (Actb) promoter-driven Flp recombinase (to remove the neomycin resistance gene *via* FRT site recombination) or an Mx2 promoter-driven Cre recombinase (to remove METTL14 exons 7–9, as well as the included neomycin gene and FRT sites, *via* loxP site recombination). Offspring from the Actb-Flp cross harbor a *Mettl14* gene whose sixth through ninth exons are loxP-flanked (floxed), allowing for subsequent Cre-mediated deletion of the methyltransferase active site encoded within exon 7. Mice homozygote for the loxP site was crossed to a transgenic line with Cre-recombinase under control of rat insulin-2 promoter.

### 2.12. In vivo characterization of mice

*Mettl14$^{flox/flox}$* mice in mix background were used for experiments. The mice were usually fed a normal chow (NC) diet (Teklad Global 18% Rodent Diet 2018; Harlan Teklad) and maintained in a standard 12 light/12 dark cycle. Male mice were placed on either regular diet or a high-fat diet containing 42% fat (TD.88137; Harlan Teklad) from 4 weeks of age and provided with water *ad libitum* as previously described [25]. Intraperitoneal glucose tolerance tests were performed on mice after a 5-hour fast (2 g/kg dextrose) at age of 15 weeks for normal chow mice or 12 weeks after HFD. Body weight was monitored weekly. Total body fat content was quantified using dual energy X-ray absorptiometry (DEXA) scans (Lunar PIXImus II, Madison, WI) under anesthesia. Indirect calorimetric measurement was carried out using the LabMaster System (TSE Systems, Midland, MI), and oxygen consumption, $CO_2$ production, energy expenditure, food and water intake, and locomotive movement were recorded for 4 days following a 3-day acclimation. Insulin levels were measured at 0 and 10 min after glucose challenge. Insulin tolerance tests were performed after a 5-hour fast by administering human recombinant insulin (0.75 U/kg). We quantified β-cell area from anti-insulin–stained pancreas sections counterstained with hematoxylin using the intensity thresholding function of the integrated morphometry package in ImageJ. The relative β-cell area was measured from anti-insulin–stained pancreas sections counterstained with hematoxylin using ImageJ software. At least 10 pancreatic serial sections (6 μm) spaced 50 μm apart per block were stained for each animal ($n$ = 3 mice of each group). The ratio of stained islet to the pancreas was calculated and these same measurements on at least 10 sections were performed. At last, the average β-cell mass was calculated by multiplying the β-cell area: pancreas area ratio X the pancreatic weight. Ki-67 staining was performed as previously described [25,26]. For Ki67 staining, at least 10,000 β-cells were counted per mouse. For TUNEL staining, > 10,000 β-cells were counted. All animal experiments in this study were performed under protocols approved by the University of Chicago Animal Studies Committee and were conducted in accordance with National Institutes of Health guidelines for the care and use of animals in research.

#### 2.12.1. Imaging studies of pancreatic islets

Formalin-fixed pancreas sections underwent antigen retrieval in boiling citrate buffer (pH 6.0) for 10 min before labeling with antibodies against insulin (A0564; DAKO), glucagon (G2654; Sigma-Aldrich), and DAPI (P-36931; Invitrogen).

### 2.13. Statistical analysis

The 2-tailed unpaired Student's *t*-test was used to assess the statistical significance of differences between 2 sets of data. Differences were considered significant when $P < 0.05$. In all experiments, the number of asterisks is used to designate the following levels of statistical significance: $***P < 0.001$, $**P < 0.01$, $*P < 0.05$ compared with control group or *Mettl14$^{+/+}$Cre$^{+}$* (*WT*) group. Results are presented as mean ± SEM. Each experiment was repeated three times.

## 3. Results

### 3.1. Rip-driven Mettl14 deletion in β-cells leads to glucose intolerance and decreases insulin secretion

First, we determined whether METTL14 deficiency (KD) affects the ratio of m$^6$A/A in mRNA in MIN6 cells. The results showed that METTL14 knockdown (KD) induced a decreased ratio of m$^6$A/A in mRNA by 36.8% (Fig. 1.A). To define the role of METTL14 in β-cells *in vivo*, we set up the crosses of global heterozygous mice and obtained 73 live born pups. Of these mice, 39 were wild type, 34 were heterozygous, and 0 was homozygous for *Mettl14*, indicating that complete loss of *Mettl14* is embryonic lethal. Thus in order to determine the role of *Mettl14* in β-cells, we generated conditional β-cell *Mettl14* knockout mouse lines using rat Ins2 promoter-Cre (*RIP-Cre*, *βKO*) (sup Fig. 1). Considering that a large amount of mRNA are methylated inside mammalian cells, the overall global decrease in m$^6$A mRNA methylation could have significant effects on cellular physiology, thus we next examined whether the reduced m$^6$A methylation affects *β*-cell function. To our test, we found that on normal chow, *βKO* mice at 4 weeks old had lower body weight compared to *WT* littermates (*Mettl14$^{+/+}$Cre$^{+}$*, *WT*) mice by 35% in male (Fig. 1.B and C) and 26% in female (sup 2.A and B), respectively ($P < 0.01$). Interestingly, the body weight was comparable after 5 weeks old between the *βKO* mice and control littermates (Fig. 1.B and sup Fig. 2.A). Given the critical role of β-cells in metabolism, we assessed the metabolic profile of *βKO* mice. On normal chow, these mice had similar feeding and fasting serum glucose levels (Fig. 1.D and sup Fig. 2.C), however, both male and female *βKO* mice revealed glucose intolerance during glucose tolerance test (GTT) compared to control littermates (Fig. 1.E and F). Glucose concentrations following intraperitoneal glucose were significantly higher in both male and female *βKO* mice compared to *WT* mice (Fig. 1.E and F). The area under the blood glucose curve (AUC) was increased by 77.8% ($P < 0.001$) in male and 120.8% ($P < 0.001$) in female *βKO* mice compared to control littermates (Fig. 1.E and F). We also found that even 4-week old *βKO* mice were glucose intolerant (Fig. 1.G and sup Fig. 2.D). To determine whether the higher glucose levels in *βKO* mice are related to insulin secretion defect, we determined the insulin

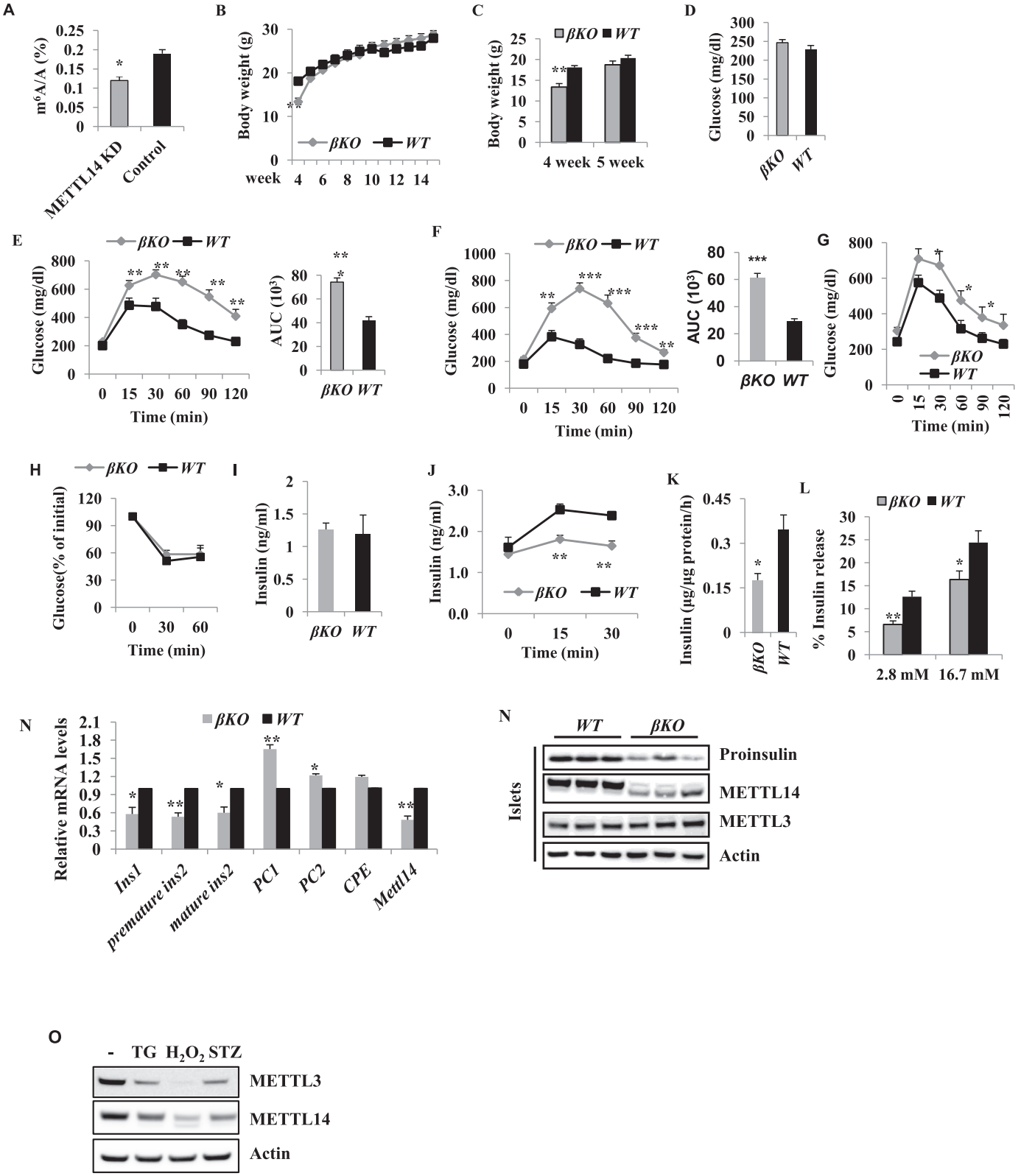


*(caption on next page)*

concentration. The results showed that feeding insulin levels were comparable between the *βKO* mice and control littermates (Fig. 1.H, I). However, the plasma insulin levels were significantly lower in *βKO* mice than those in the control mice at 15 and 30 min (both $P < 0.01$) after glucose challenge (Fig. 1.J). Glucose-stimulated insulin secretion (GSIS) from isolated islets was also measured, and we found that isolated size-matched islets from *βKO* mice released less insulin (Fig. 1.K) and the ratio of insulin secretion was also reduced in response to glucose stimulation (Fig. 1.L). Since reduced insulin expression may also contribute to insufficient insulin secretion, we determined the expression levels of insulin in islets from *WT* and *βKO* mice. The mRNA levels of *Ins1*, *Premature Ins2*, *Ins2*, *PC1* and *CPE* ($P < 0.05$ or

**Fig. 1.** The phenotype of *βKO* mice. (A) The ratio of $m^6A/A$ in purified mRNA. 3 days after Mettl14 KD, $m^6A$ percentage is determined by liquid chromatography tandem mass spectrometry. *$P < 0.05$. (B + C) Body weights of male mice. (D) Feeding glucose levels in 12-week old male mice with regular chow diet. (E + F) Blood glucose levels after intraperitoneal injection of dextrose (2 g/kg) in the 15-week old male (E) and female mice (F) with regular chow diet. Area under the blood glucose curves (AUC) using the data from left in the mice. (G) Blood glucose levels after intraperitoneal injection of dextrose (2 g/kg) in 4-week old male mice fed a regular chow diet. (H) Glucose levels in response to 0.75 U/kg body weight insulin in 15-week old male mice. (I) Random feeding blood insulin levels in the 16-week old male mice. (J) Insulin levels measured at 0, 15 and 30 min after intraperitoneal dextrose in 17-week old male mice. (K + L) Insulin release in isolated islets from 12-week old mice ($n = 3$). Insulin release in the isolated islets from 12-week old female mice in presence of 16.7 mM (K) glucose or 2.8 and 16.7 mM glucose (L) for 1 h. (M) Quantitative RT-PCR analysis of expression levels of a number of genes involved in the insulin secretory pathway in islets. (N) Protein levels of proinsulin, METTL14, METTL3 and Actin in isolated islets from the 12-week old mice. Each lane represents an individual mouse. All the mice above are fed on normal chow diet. (O) Effect of β-cell damage reagents on METTL14 levels. The islets were isolated from 6 to 8 week C57/B6 male mice and treated with 50 μM $H_2O_2$, 1 μM thapsigargin and 1 mM STZ for 4 h. METTL14 and METTL3 protein levels were determined by Western blot. Values are mean ± SEM. *$P < 0.05$, **$P < 0.01$, ***$P < 0.001$ compared to *WT* mice. $n = 12$–22.

$P < 0.01$) were significantly decreased in islets from *βKO* mice, but mRNA levels of glucagon were similar in *βKO* and *WT* mice (Fig. 1.M). The protein levels of proinsulin were also decreased in islets from *βKO* mice (Fig. 1.N). Interestingly, METT3 levels were slightly increased rather than decreased in *βKO* islets (Fig. 1.N). To determine whether there is a correlation between β-cell damage/dysfunction and β-cell METTL14 levels, we isolated the islets from 6 to 8 week old C57/B6 male mice, and treated the islets with 50 μM $H_2O_2$, 1 μM thapsigargin and 1 mM STZ for 4 h. The results showed that both METTL14 and METTL3 were dramatically decreased after these stimuli (Fig. 1.O). These results indicate that *βKO* mice have less insulin secretion and less insulin expression in β-cells. β-Cell damage may decrease METTL14 expression.

### 3.2. Decreased β-cell mass in βKO mice is related to the increase in β-cell death and the defect in β-cell differentiation

To determine the mechanism for the reduced insulin release described above, we examined the morphology of the pancreatic islets. Histological analysis of the *βKO* pancreas indicated that mutant islets are smaller and more disorganized than those in *WT* littermate controls (Fig. 2.A). However, the ratio of β-cells/α-cells was similar in islets from the *WT* and *βKO* mice (sup Fig. 2.E). We also found that β-cell mass in *βKO* mice was reduced by 31.1% ($P < 0.05$) compared to *WT* mice (Fig. 2.B). To determine whether reduced β-cell mass in *βKO* mice is related to increased β-cell death and/or decreased β-cell proliferation, we measured β-cell death and proliferation by TUNEL staining and Ki67+ labeling, respectively. β-Cell death in *βKO* islets was significantly increased (Fig. 2.C) and proliferation was similar between *βKO* and *WT* islets (Fig. 2.D).

Given RIP-Cre is expressed in early stage during pancreas development and the transcription factors are very important in β-cell development, we evaluated the mRNA levels of key transcription factors. The results showed that expression levels of Pdx1 ($P < 0.01$) and HNF4α ($P < 0.05$) were significantly decreased in *βKO* islets, while Neurod1, Nkx6.1 and Pax6 did not change much (Fig. 2.E). Both Pdx1 and HNF4 α mRNAs have $m^6A$ peak at 3′ UTR (Fig. 2.F). Moreover, we found that *βKO* neonates and younger mice were smaller than *WT* mice (Fig. 2.G), which is consistent with the result in Fig. 1.A. Together, these results suggest that METTL14 may play an important role in β-cell development. To confirm this hypothesis, we examined the markers of endocrine progenitors in pancreas. Western blot confirmed that Neurogenin3 (Ngn3) and Sex determining region Y-box 2 (Sox2) were significantly increased in *βKO* β-cells (Fig. 2.H).

Octamer-binding transcription factor 4 (Oct4) was undetectable in both WT and *βKO* β-islets (Fig. 2.H). Some cells stained positive for both glucagon and insulin in βKO islets (Fig. 2.I), suggesting that endocrine progenitors could not fully differentiate into mature α or β-cells [27]. The results above indicate that METTL14 deficiency in β-cells induces β-cell death and defects in β-cell differentiation, resulting in lower beta cell mass and lower insulin secretion.

To further confirm these results, METTL14 was knocked down in MIN6 cells by lentiviral shRNA. First, we determined the net cell number after METTL14 KD in MIN6 cells. The results showed that the net cell number was decreased by 48% in METTL14 KD cells ($P < 0.001$, Fig. 3.A). The results showed that METTL14 knockdown (KD) induced a significant increase in cell death and cleaved caspase 3, and a decrease in METTL3 (Fig. 3.B). The percentage of cells stained positive for PI was 11.9 ± 9.3% in control cells and 54.1 ± 0.4% ($P < 0.001$) in METTL14 KD cells on day 3 (Fig. 3.C), and the percentage of cells staining positive for TUNEL was 1.7-fold greater in METTL14 KD cells than in control cells (Fig. 3.D). Z-VAD, a pan-caspase inhibitor, significantly inhibited the increase in cleaved caspase 3 induced by METTL14 KD in MIN6 cells (Fig. 3.E). In addition, Z-VAD significantly increased the net cell number and decreased the cell death induced by METTL14 KD (Fig. 3.E). The cell death induced by METTL14 suppression was related to the decrease in Bcl-xL and the increase in Bim (Fig. 3.F). Overexpression of Bcl-xL not only efficiently induced a decrease in cleaved caspase 3 and cell death but also induced an increase in net cell number (Fig. 3.G). These results indicate that β-cell death induced by METTL14 deficiency is related to the changes in molecules that regulate the rate of apoptosis.

### 3.3. βKO mice on HFD are glucose intolerance but have enhanced whole body insulin sensitivity

We further evaluated metabolic profiles of the *βKO* mice maintained on a HFD. On a normal chow diet, body weight and whole body fat content was similar in *βKO* and *WT* mice. However, on HFD, the body weight of the *βKO* mice was lower than that of control mice (Fig. 4.A), and whole body fat content was 19.7% higher in *βKO* mice ($P < 0.05$, Fig. 4.B). Random feeding and overnight-fasting glucose levels were comparable between *βKO* and *WT* mice with HFD-feeding (Fig. 4.C), which is consistent with normal chow condition. Again, glucose concentrations during GTT were higher in the *βKO* mice. The AUC was increased by 44.2% ($P < 0.01$) in the *βKO* mice compared to *WT* mice (Fig. 4.D). The feeding insulin level was significantly lower in *βKO* mice ($P < 0.05$) (Fig. 4.E). The insulin secretion following glucose challenge in *βKO* mice was less than in *WT* mice (Fig. 4.F). Surprisingly, *βKO* mice on HFD were more insulin sensitive as demonstrated by greater lowering of glucose levels during insulin tolerance test (ITT) (Fig. 4.G). The AUC of insulin response was 30.3% lower in *βKO* mice than in *WT* mice (Fig. 4.G). To determine whether Mettl14 deficiency impair compensatory islet expansion during HFD feeding, the β-cell mass was measured in *WT* and *βKO* mice on HFD for 14 weeks. Compared to normal chow, HFD induce a 2.3-fold increase in β-cell mass from 0.45 ± 0.06 mg in normal chow to 1.52 ± 0.07 mg in HFD in βKO mice, much less than the 3.4-fold increase in β-cell mass from 0.67 ± 0.04 mg in normal chow to 2.93 ± 0.46 mg in HFD in WT mice (Fig. 3.H). Compared to *WT* mice, there is no significant difference in β-cell death but significant decrease in β-cell proliferation in *βKO* mice on HFD ($P < 0.05$, Fig. 4.H). These results indicate that METTL14 deficiency impair compensatory islet expansion on HFD feeding, which is one of the reasons that *βKO* mice develop diabetes. The heat production and the mean respiratory exchange ratio (RER) were comparable between the *βKO* mice and control littermates (Fig. 4.I and J). *βKO*

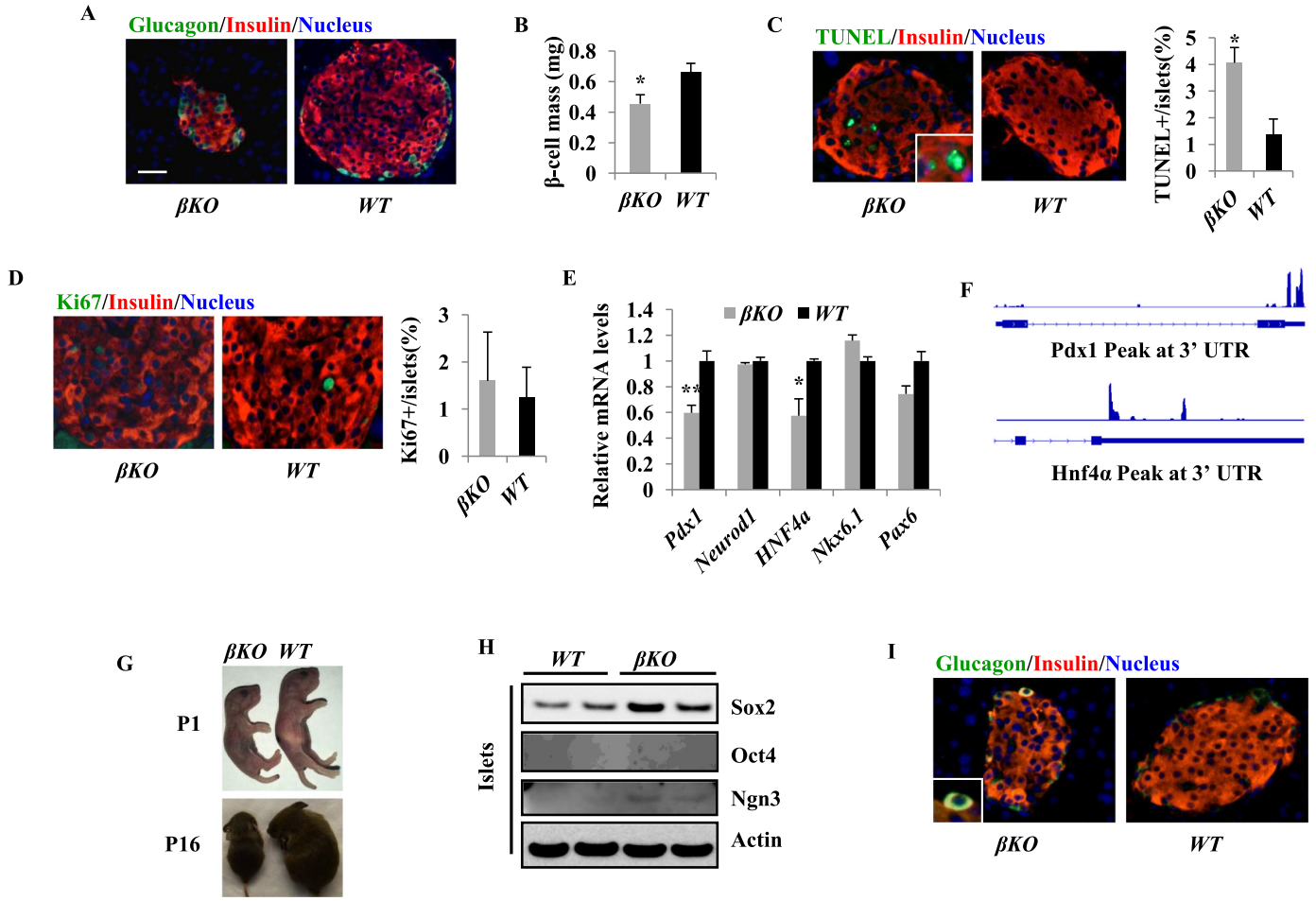


**Fig. 2.** *Mettl14* ablation in *βKO* mice with normal chow decreases β-cell mass related to the increase in cell death and the defect in β-cell development. (A) Islet morphology in 17-week old mice. Anti-insulin and anti-glucagon antibodies were used to stain β-cells (red) and α-cells (green), respectively. Nuclei were stained with DAPI (blue). The scale bar represents 20 μm. (B) β-cell mass in 18-week old *βKO* mice ($n$ = 3–5 per group). (C + D) TUNEL staining and Ki67$^+$ labeling of pancreatic β-cells from 17-week old mice. Quantitative TUNEL (C) and Ki67$^+$ β-cells (D) data are shown ($n$ = 3–5 per group). Original magnification, X200. (E) Quantitative RT-PCR analysis of gene expression levels in islets from 8 to 10 week old mice ($n$ = 3–5 per group). All the mice are fed on normal chow diet. Values are mean ± SEM. *$P$ < 0.05, **$P$ < 0.01 compared to *WT*. (F) m$^6$A methylation and transcriptional landscape. M$^6$A-seq analysis shows m$^6$A enrichment in some genes in MIN6 cells. (G) Day 1 and Day 16 after birth, *βKO* mice exhibit smaller body size. (H) Protein levels of Sox2, Oct4 and Ngn3 in islets isolated from 8 to 10 week old mice. Each lane represents one group of mice, ($n$ = 3–5 mice per group). (I) Islet morphology in 17-week old mice described as above (A).

mice exhibited lower physical activity and food intake during the day time (both $P$ < 0.05, Fig. 4.K and L).

### 3.4. βKO mice on HFD exhibit increased insulin sensitivity in liver

The potential role of the liver in the improved insulin sensitivity in *βKO* mice on HFD was examined. We found that the liver weights of *βKO* mice with HFD were 82.8% lower ($P$ < 0.05) than those of *WT* mice (Fig. 5.A). Furthermore, fat accumulation in the livers of *βKO* mice was significantly decreased (Fig. 5.B), and the liver triacylglycerol levels in *βKO* mice were decreased by 31.8% ($P$ < 0.01) (Fig. 5.C). Consistently, expression of the major *de novo* lipogenesis enzymes acetyl-CoA carboxylase (ACC) and fatty acid synthase (FASN) was significantly decreased, and the mRNA level of lipolysis enzyme adipose triglyceride lipase ATGL were dramatically increased in the liver of *βKO* mice (Fig. 5.D). In addition, we evaluated phosphorylated Akt (p-Akt) levels in the liver and found that p-Akt was higher in the liver of *βKO* mice compared to *WT* mice in the presence of insulin (Fig. 5.E). We further measured the plasma glucagon, another humoral factor regulating glucose levels, and found that the plasma glucagon was unchanged in the *βKO* mice compared to *WT* mice (Fig. 5.F). To further analyze insulin sensitivity in the liver, we performed pyruvate tolerance test (PTT) on mice. Glucose concentrations following pyruvate challenge were significantly decreased in *βKO* mice (Fig. 5.G), consistent with a reduction in hepatic gluconeogenesis which is related to the decrease in mRNA levels of G6Pase and PEPCK (Fig. 5.H). These results suggest that *βKO* mice have enhanced responsiveness to insulin associated with the decrease in fat accumulation and gluconeogenesis, and the enhanced insulin signaling in liver.

### 3.5. Mettl14 deficiency alters gene expression in β-cells

To investigate the mechanism underlying how *Mettl14* regulates β-cell function, we performed RNA sequencing (RNA-seq) to detect gene expression changes in *βKO* islets from mice fed on normal chow. The results showed that expression levels of 878 transcripts were altered (547 upregulated *vs* 331 downregulated) in islets from *βKO* mice compared to those from control mice. Among those altered genes, 169 genes were significantly upregulated ($P$ < 0.001) and 41 genes were significantly downregulated ($P$ < 0.001). Notably, we found significant increase in mRNA levels of Reg2 (regenerating islet-derived 2, q = 0.0053) and Reg1 (regenerating islet-derived 1, q = 0.0053), both of which are important for regeneration of β-cells. qRT-PCR confirmed that Reg1 and Reg2 were upregulated by 2.0-fold and 1.1-fold,

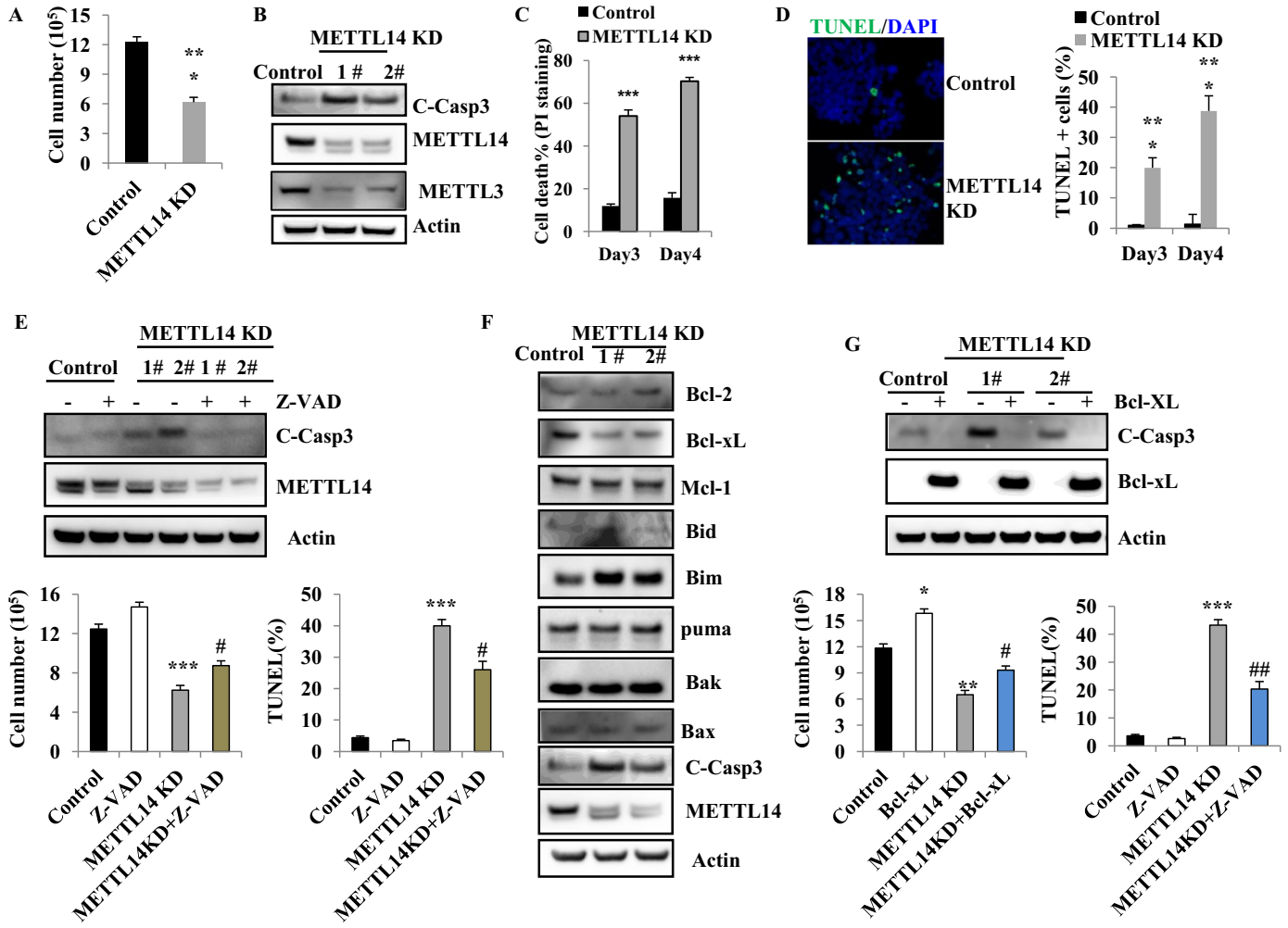


**Fig. 3.** Bcl-2 family members are involved in METTL14 KD induced beta cell death. (A) The net cell number was measured in METTL14 KD cells 4 days after METTL14 KD. (B) Protein levels of cleaved caspase 3 in MIN6 cells 4 days after Mettl14 KD using two different shRNA lentivirus (n = 3). (C) Cell death was determined by PI-staining in MIN6 cells after Mettl14 KD. (D) TUNEL labeling of METTL14 KD MIN6 cells. 3 days after infection with METTL14 shRNA lentivirus, apoptotic cells were assayed by TUNEL staining. Quantitative TUNEL data are shown. (E) Z-VAD inhibits caspase3 cleavage induced by METTL114 KD. MIN6 cells were treated with the caspase inhibitor Z-VAD (20 μM), for 2 h prior to infection with METTL14 shRNA lentivirus. 4 days later, cleaved caspase3 protein was assayed by Western blot. The net cell number and TUNEL staining were also measured ($n$ = 3). (F) Protein levels of Bcl-2 family members in MIN6 cells 4 days after Mettl14 KD. (G) Effect of overexpression of Bcl-xL on the cleavage of caspase3. MIN6 cells were infected with METTL14 shRNA lentivirus and retrovirus overexpressing Bcl-xL for 3 days, then protein levels of cleaved caspase3 and Bcl-xL were determined by Western blot. The net cell number and TUNEL staining were also measured ($n$ = 3).

respectively (Fig. 6.A). Moreover, we found mRNA levels in numerous genes that play an important role in cell death were increased, including Tnfrsf1a (TNF receptor superfamily member 1a), Tnfrsf11b (TNF receptor superfamily member 11b), C9 (complement factor 9), Gsdma (gasdermin-A), Ern1 (endoplasmic reticulum to nucleus signaling 1), Fgl2 (fibrinogen-like protein 2), Gas2 (growth arrest-specific protein 2), Ngfr (nerve growth factor receptor), Plg (plasminogen) (Fig. 6.B). The upregulated genes related to cell death, such as Ern1α, Fgl2, Ngfr and Plg in *βKO* islets were confirmed by qRT-PCR (Fig. 6.C and E). Plg was increased by 360-fold in *βKO* islets compared to *WT* islets (Fig. 6.C). The sets of genes showing consistent upregulation are enriched for GO term analysis related to acute inflammatory response and inflammatory response (Fig. 6.D). Furthermore, we validated a number of genes related to acute inflammatory response: Ptger3 (Prostaglandin E Receptor 3) and F2 (coagulation Factor II) were upregulated by 7-fold; Orm1 (orosomucoid 1), Tnfrsf1a, Saa1 (serum amyloid a1), Saa2 (serum amyloid a2) and Trf (transferring) were increased by 30 to 130-fold; C3 (complement factor 3) and C9 were induced by 17 and 495-fold, respectively (Fig. 6.E). We also found that most of these genes have m$^6$A peak in MIN6 cells (Fig. 6.F). Unfortunately, we cannot get enough mRNA from islets for m$^6$A immunoprecipitation in order to directly detect levels of m$^6$A methylation on each transcript in β-cells. Taken together, the changes in expression levels of these genes indicate that METTL14 deficiency is associated with the increase in both β-cell death and the inflammatory response.

## 4. Discussion

m$^6$A modification has been implicated in mRNA stability, turnover, localization, and translation efficiency [28]. An enzyme complex composed of METTL3, METTL14 and WTAP generates m$^6$A on mRNAs. Recently, METTL14 or METTL3 KD-induced cell death has been reported in other cell types such as Hela [20,29]. Indeed, the levels of m$^6$A were significantly decreased in METTL14 KD MIN6 cells. *βKO* mice showed glucose intolerance and decreased insulin secretion due to the reduction of β-cell mass. Moreover, we found that METTL14 levels were decreased after β-cell damage reagent stimulation. The results indicate that there is a correlation between β-cell METTL14 levels and β-cell damage. Our results indicate that β-cell death contributes to the lower β-cell mass in *βKO* mice on normal chow. Whether defects in β-cell development contribute to the lower β-cell mass in *βKO* mice need to be

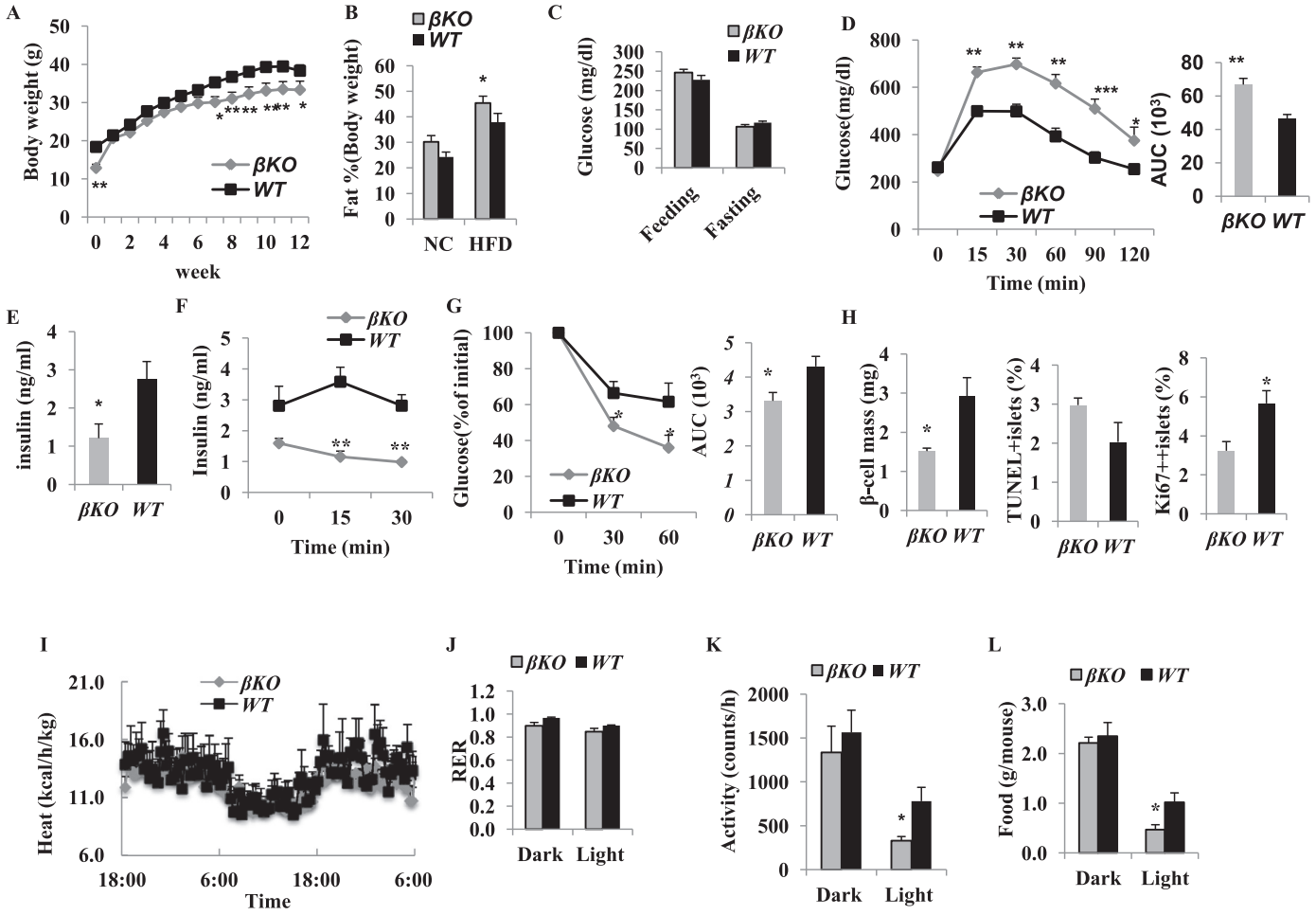


**Fig. 4.** *βKO* mice on HFD are glucose intolerant but have enhanced insulin sensitivity. (A) Body weight of male mice on HFD. The male mice were fed on HFD at 4-weeks old and the body weight was measured. (B) Whole body fat content of male mice on HFD for 15 weeks. (C) Random feeding and fasting (overnight) blood glucose levels in male mice on HFD for 13 weeks. (D) Blood glucose levels and AUC after intraperitoneal injection of dextrose (1 g/kg) in male mice on HFD for 12 weeks. (E) Feeding blood insulin levels in male mice on HFD for 13 weeks. (F) Insulin levels measured at 0, 15 and 30 min after intraperitoneal dextrose (1 g/kg) in male mice on HFD for 13 weeks. (G) Glucose levels and AUC in response to 0.75 U/kg body weight insulin in male mice on HFD for 12 weeks. (H) β-Cell mass, β-cell death and proliferation were determined in mice on HFD for 14 weeks. (I–J) heat production (I), respiratory exchange ratio (RER, J), activity (K) and food intake (L) were measured between *βKO* and *WT* mice on HFD for 16 weeks. Values are mean ± SEM. $^{*}P < 0.05$, $^{**}P < 0.01$, $^{***}P < 0.001$ compared to *WT* mice. $n = 10–14$.

further investigated. Since METTL14 has been demonstrated that it can forms stable heterodimer with METTL3 [28], we assume that METTL14 deficiency will decrease METTL3 levels. Indeed, METTL14 KD in MIN6 cells decreased METTL3 levels. However, METTL3 levels were slightly increased instead decreased in METTL14 deficient islets. One explanation to this result is that both METTL14 deficient beta cells with decreased METTL3 level have been dead and cleaned. Only beta cells with normal or slightly increased METTL3 were survival and kept in islets. Thus we cannot detect decreased METTL3 in METTL14 deficient islets. Another explanation is that increased METTL3 is the results of compensation in METTL14 deficient islets in order to maintain β-cell function. METTL3/14 is found in the nucleus where it is localized to nuclear speckles and WTAP is required for this nuclear localization pattern [12]. Although the function of METTL3/14-WTAP complex is not fully understood, METTL3/14 and WTAP may affect each other. The decreased METTL14 may upregulate METTL3 by unknown mechanism as secondary effects in islets, which can explain the modest phenotype of *βKO* mice.

Our gene ontology (GO) analysis also showed that some genes related to cell death such as Ern1α, Ggl2, Ngfr and Plg were altered in *βKO* islets, which may contribute to METTL14 deficiency-induced β-cell death. In addition, we found that upregulated mRNAs such as C3 and C9 in *βKO* islets were enriched in acute inflammatory response. Both effector and regulatory/inhibitory components of the complement system are upregulated in pancreas from patients with type 1 diabetes [30]. C3-deficient mice and mice with hematopoietic cell-specific C3 deficiency are protected from development of insulitis and diabetes [31].

By qRT-PCR on isolated islets, we found downregulation of Hnf4α and Pdx1 in *βKO* islets. Hnf4α regulates the expression of β-cell genes involved in glucose metabolism and nutrient-induced insulin secretion. Mutations in the *HNF4α* gene are associated with MODY1, which is characterized by impaired insulin secretory response to glucose in pancreatic β-cells [32]. Pdx1, a critical transcription factor in β-cells maintains β-cell identity [33], regulates early pancreas formation [34], insulin secretion [35], mitochondrial metabolism [36], cell survival [25,37], the expression of the insulin gene and other components of the glucose-stimulated insulin secretion pathway [9]. Thus downregulation of Hnf4α and Pdx1 in *βKO* islets will result in defect in maintaining β-cell identity, an increase in β-cell death, and a decrease in β-cell mass and insulin secretion. Since insulin regulates early growth [38], the decreased insulin secretion in *βKO* mice may contribute to the lower body weight of *βKO* at the earlier age such as 4-week old.

Another interesting finding is that insulin sensitivity was increased

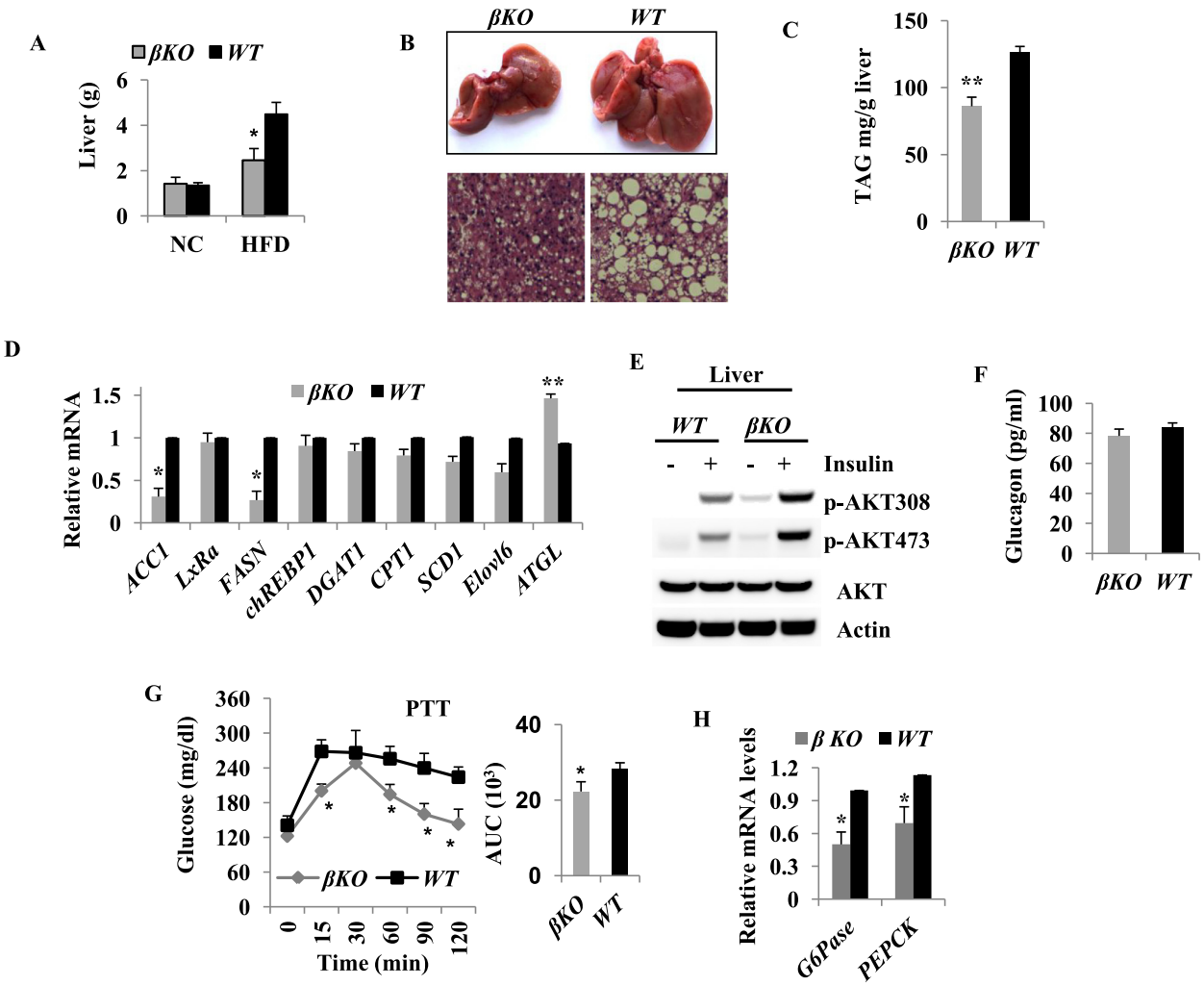


**Fig. 5.** *βKO* mice on HFD exhibit increased insulin sensitivity in liver. (A) Liver weights of male mice on normal chow for 6 months and HFD for 5 months. (B) Livers and HE staining of liver from male mice on HFD for 5 months. (C) triacylglycerol levels in male mice on HFD for 5 months. (D) mRNA levels in the liver of male mice on HFD for 5 months after overnight fasting. (E) AKT activity in the liver. The male mice (4 weeks) were fed a HFD for 5 months, fasted for 20–24 h, and injected with insulin (2 units/kg body weight) *via* inferior vena cava. Liver extracts were prepared 5 min after insulin stimulation and immunoblotted with antibodies against phospho-Akt (pThr308 and pSer473) or Akt. (F) Blood glucagon levels in male mice on HFD for 4 months. (G) Pyruvate tolerance test (pyruvate: 2 g/kg) in male mice on HFD for 5 months after fasting overnight. (H) Expression levels of G6Pase and PEPCK in the liver from male mice on HFD for 5 months after fasting overnight. Values are mean ± SEM. $^{*}P < 0.05$, $^{**}P < 0.01$ compared to *WT*. $n = 8–14$.

in *βKO* mice on HFD, which is related to the increase in insulin signaling, and the decrease in fat accumulation and gluconeogenesis in the liver. Although insulin sensitivity was increased, the glucose levels were still higher after 2 h of glucose injection in *βKO* mice on HFD, which suggest that insulin sensitivity could not fully compensate for insulin secretion reduction in *βKO* mice. The reduction in insulin secretion in *βKO* mice is related to decreased β-cell mass. METTL14 deficiency impairs compensatory islet expansions on HFD feeding.

In this study, we found that 547 transcripts were upregulated and 331 transcripts were downregulated among the altered transcripts in islets from *βKO* mice. Studies on cultured cell lines have established that one important effect of m$^6$A methylation was to decrease RNA stability due to accelerated decay [23]. Although there are some genes indeed have m$^6$A sites in MIN6 cells, unfortunately, we cannot directly detect levels of m$^6$A methylation on each transcript in primary β-cells due to technical limit. Previous studies suggest that m$^6$A mediated mRNA decay operates through YTHDF2 as a major pathway in transcriptome switching during cell differentiation and development [39–41]. Up-regulation of mRNAs after *Mettl14* deletion was expected, but downregulation of mRNAs was surprising. It remains to be determined if downregulation of mRNAs after *Mettl14* deletion is due to unique functions of m$^6$A methylation in β-cells mediated through other reader proteins or caused by secondary effects following chronically altered β-cell functions due to *Mettl14* deficiency.

In summary, our data are the first to show that Mettl14 is essential for β-survival, differentiation and insulin secretion. METTL14 deficiency in β-cells increased cell death, altered cell differentiation, and decreased β-cell mass and insulin secretion, leading to glucose intolerance. Our finding suggests that METTL14 could be a promising target for diabetes treatment. Major challenges remain in determining how m$^6$A and its reader proteins (*e.g.* YTHDF1, YTHDF2, and/or other readers) dynamically regulate β-cell mass and temporal control of protein synthesis in response to stress during diabetes.

## Author contributions

D.R. conceived and designed experiments. J.L., G. L., J.S., L.M., Y.H., performed the experiments. G.L., C.H., D.R. performed data analysis and bioinformatics. D.R. wrote the manuscript. All authors contributed to interpretation of data and final writing of the manuscript.

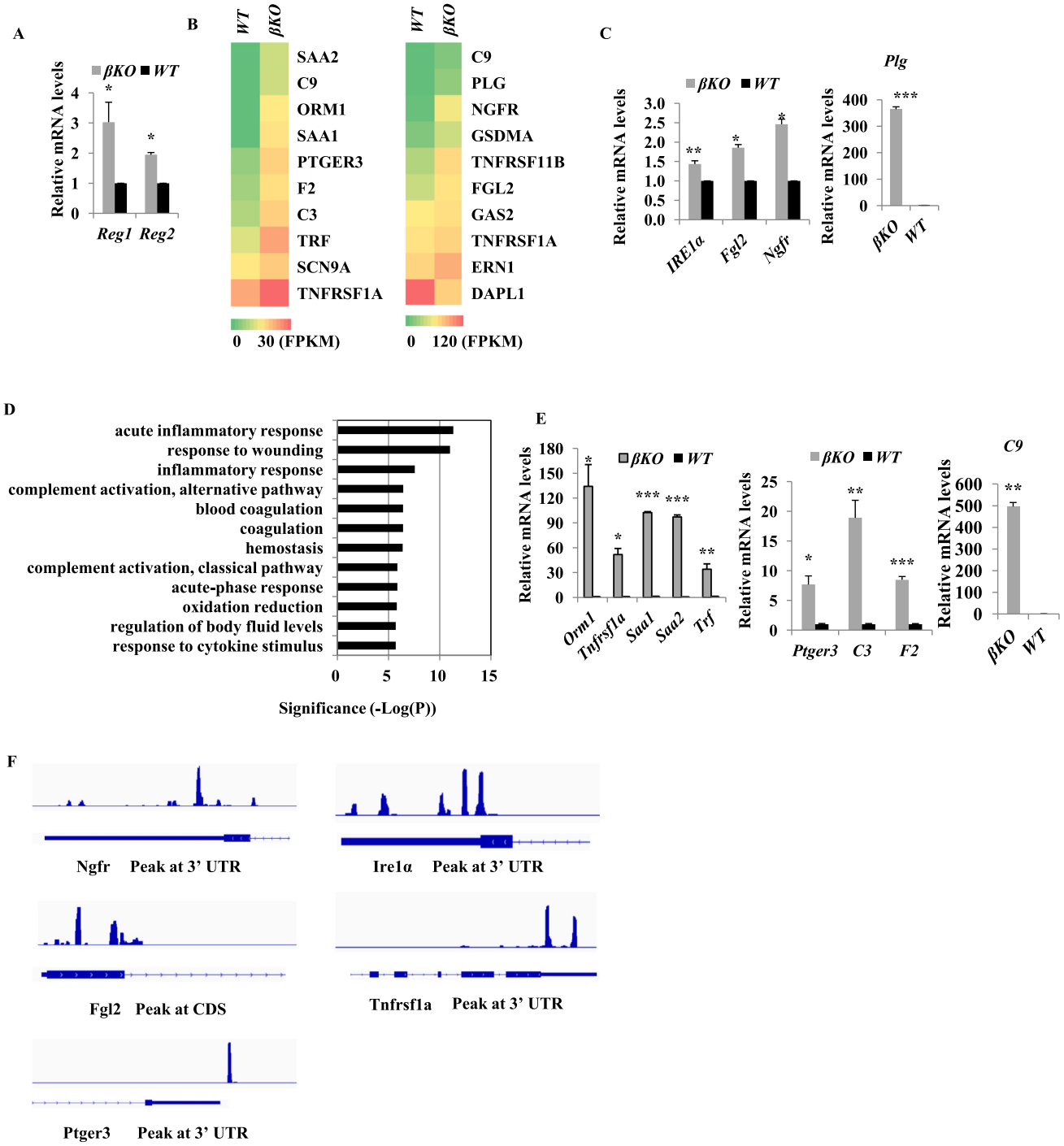


**Fig. 6.** Gene microarray analysis of *βKO* mice with normal chow. (A) (A–C, E) Validation of genes by real-time qRT-PCR in islets from 8 to 9 week old male mice. (D) Cluster analysis of significantly (FDR < 0.1) altered genes (mRNA transcripts) in islets from 8 to 9 week old male mice. (F) $m^6A$ methylation and transcriptional landscape. $M^6A$-seq analysis shows $m^6A$ enrichment in some genes in MIN6 cells. $^*P < 0.05$, $^{**}P < 0.01$, $^{***}P < 0.001$ compared to *WT*. $n = 3–5$.

## Transparency document

The Transparency document associated this article can be found, in online version.

## Acknowledgements

The authors thank Dr. Kenneth Polonsky for insightful suggestions, advice and discussions. This study was supported by P30-DK020595 (The University of Chicago, Diabetes Research and Training Center).

## Competing interests

No potential conflicts of interest relevant to this article were reported.

## Appendix A. Supplementary data

Supplementary data to this article can be found online at https://doi.org/10.1016/j.dummy.2019.01.002.

## References


[1] J.D. Rivas-Carrillo, T. Okitsu, N. Tanaka, N. Kobayashi, Pancreas development and beta-cell differentiation of embryonic stem cells, Curr. Med. Chem. 14 (2007) 1573–1578.

[2] C. Bernard-Kargar, A. Ktorza, Endocrine pancreas plasticity under physiological and pathological conditions, Diabetes 50 (Suppl. 1) (2001) S30–S35.

[3] L. Scaglia, C.J. Cahill, D.T. Finegood, S. Bonner-Weir, Apoptosis participates in the remodeling of the endocrine pancreas in the neonatal rat, Endocrinology 138 (1997) 1736–1741.

[4] D.T. Finegood, L. Scaglia, S. Bonner-Weir, Dynamics of beta-cell mass in the growing rat pancreas. Estimation with a simple mathematical model, Diabetes 44 (1995) 249–256.

[5] M. Teta, S.Y. Long, L.M. Wartschow, M.M. Rankin, J.A. Kushner, Very slow turnover of beta-cells in aged adult mice, Diabetes 54 (2005) 2557–2567.

[6] T. Miyatsuka, Chronology of endocrine differentiation and beta-cell neogenesis, Endocr. J. 63 (2016) 205–211.

[7] M. Teta, M.M. Rankin, S.Y. Long, G.M. Stein, J.A. Kushner, Growth and regeneration of adult beta cells does not involve specialized progenitors, Dev. Cell 12 (2007) 817–826.

[8] A.M. Ackermann, M. Gannon, Molecular regulation of pancreatic beta-cell mass development, maintenance, and expansion, J. Mol. Endocrinol. 38 (2007) 193–206.

[9] Z. Fu, E. R. Gilbert, D. Liu, Regulation of insulin synthesis and secretion and pancreatic Beta-cell dysfunction in diabetes, Curr. Diabetes Rev. 9 (2013) 25–53.

[10] P.V. Roder, X. Wong, W. Hong, W. Han, Molecular regulation of insulin granule biogenesis and exocytosis, Biochem. J. 473 (2016) 2737–2756.

[11] T. Pan, N6-methyl-adenosine modification in messenger and long non-coding RNA, Trends Biochem. Sci. 38 (2013) 204–209.

[12] Y. Yue, J. Liu, C. He, RNA N6-methyladenosine methylation in post-transcriptional gene expression regulation, Genes Dev. 29 (2015) 1343–1355.

[13] Y. Niu, X. Zhao, Y.S. Wu, M.M. Li, X.J. Wang, Y.G. Yang, N6-methyl-adenosine (m6A) in RNA: an old modification with a novel epigenetic function, Genomics Proteomics Bioinforma. 11 (2013) 8–17.

[14] B. Huisman, G. Manske, S. Carney, S. Kalantry, Functional dissection of the m6A RNA modification, Trends Biochem. Sci. 42 (2017) 85–86.

[15] S. Geula, S. Moshitch-Moshkovitz, D. Dominissini, A.A. Mansour, N. Kol, M. Salmon-Divon, V. Hershkovitz, E. Peer, N. Mor, Y.S. Manor, M.S. Ben-Haim, E. Eyal, S. Yunger, Y. Pinto, D.A. Jaitin, S. Viukov, Y. Rais, V. Krupalnik, E. Chomsky, M. Zerbib, I. Maza, Y. Rechavi, R. Massarwa, S. Hanna, I. Amit, E.Y. Levanon, N. Amariglio, N. Stern-Ginossar, N. Novershtern, G. Rechavi, J.H. Hanna, Stem cells. m6A mRNA methylation facilitates resolution of naive pluripotency toward differentiation, Science 347 (2015) 1002–1006.

[16] J.M. Fustin, M. Doi, Y. Yamaguchi, H. Hida, S. Nishimura, M. Yoshida, T. Isagawa, M.S. Morioka, H. Kakeya, I. Manabe, H. Okamura, RNA-methylation-dependent RNA processing controls the speed of the circadian clock, Cell 155 (2013) 793–806.

[17] J. Zhou, J. Wan, X. Gao, X. Zhang, S.R. Jaffrey, S.B. Qian, Dynamic m(6)A mRNA methylation directs translational control of heat shock response, Nature 526 (2015) 591–594.

[18] P.J. Hsu, Y. Zhu, H. Ma, Y. Guo, X. Shi, Y. Liu, M. Qi, Z. Lu, H. Shi, J. Wang, Y. Cheng, G. Luo, Q. Dai, M. Liu, X. Guo, J. Sha, B. Shen, C. He, Ythdc2 is an N6-methyladenosine binding protein that regulates mammalian spermatogenesis, Cell Res. 27 (2017) 1115–1127.

[19] A. Tanabe, K. Tanikawa, M. Tsunetomi, K. Takai, H. Ikeda, J. Konno, T. Torigoe, H. Maeda, G. Kutomi, K. Okita, M. Mori, H. Sahara, RNA helicase YTHDC2 promotes cancer metastasis via the enhancement of the efficiency by which HIF-1alpha mRNA is translated, Cancer Lett. 376 (2016) 34–42.

[20] J. Liu, Y. Yue, D. Han, X. Wang, Y. Fu, L. Zhang, G. Jia, M. Yu, Z. Lu, X. Deng, Q. Dai, W. Chen, C. He, A METTL3-METTL14 complex mediates mammalian nuclear RNA N6-adenosine methylation, Nat. Chem. Biol. 10 (2014) 93–95.

[21] D. Ren, J. Sun, L. Mao, H. Ye, K.S. Polonsky, BH3-only molecule Bim mediates beta-cell death in IRS2 deficiency, Diabetes 63 (2014) 3378–3387.

[22] V. Boyd, O.M. Cholewa, K.K. Papas, Limitations in the use of fluorescein diacetate/propidium iodide (FDA/PI) and cell permeable nucleic acid stains for viability measurements of isolated islets of Langerhans, Curr. Trends Biotechnol. Pharm. 2 (2008) 66–84.

[23] X. Wang, Z. Lu, A. Gomez, G.C. Hon, Y. Yue, D. Han, Y. Fu, M. Parisien, Q. Dai, G. Jia, B. Ren, T. Pan, C. He, N6-methyladenosine-dependent regulation of messenger RNA stability, Nature 505 (2014) 117–120.

[24] J.D. Johnson, N.T. Ahmed, D.S. Luciani, Z. Han, H. Tran, J. Fujita, S. Misler, H. Edlund, K.S. Polonsky, Increased islet apoptosis in Pdx1+/− mice, J. Clin. Invest. 111 (2003) 1147–1160.

[25] D. Ren, J. Sun, C. Wang, H. Ye, L. Mao, E.H. Cheng, G.I. Bell, K.S. Polonsky, Role of BH3-only molecules Bim and Puma in beta-cell death in Pdx1 deficiency, Diabetes 63 (2014) 2744–2750.

[26] M. Chintinne, G. Stange, B. Denys, Z. Ling, P. In 't Veld, D. Pipeleers, Beta cell count instead of beta cell mass to assess and localize growth in beta cell population following pancreatic duct ligation in mice, PLoS One 7 (2012) e43959.

[27] N. Jeffery, L.W. Harries, beta-Cell differentiation status in type 2 diabetes, Diabetes Obes. Metab. 18 (2016) 1167–1175.

[28] E. Scholler, F. Weichmann, T. Treiber, S. Ringle, N. Treiber, A. Flatley, R. Feederle, A. Bruckmann, G. Meister, Interactions, localization, and phosphorylation of the m(6)A generating METTL3-METTL14-WTAP complex, RNA 24 (2018) 499–512.

[29] D. Dominissini, S. Moshitch-Moshkovitz, S. Schwartz, M. Salmon-Divon, L. Ungar, S. Osenberg, K. Cesarkas, J. Jacob-Hirsch, N. Amariglio, M. Kupiec, R. Sorek, G. Rechavi, Topology of the human and mouse m6A RNA methylomes revealed by m6A-seq, Nature 485 (2012) 201–206.

[30] R. Planas, J. Carrillo, A. Sanchez, M.C. de Villa, F. Nunez, J. Verdaguer, R.F. James, R. Pujol-Borrell, M. Vives-Pi, Gene expression profiles for the human pancreas and purified islets in type 1 diabetes: new findings at clinical onset and in long-standing diabetes, Clin. Exp. Immunol. 159 (2010) 23–44.

[31] J. Phieler, R. Garcia-Martin, J.D. Lambris, T. Chavakis, The role of the complement system in metabolic organs and metabolic diseases, Semin. Immunol. 25 (2013) 47–53.

[32] R.K. Gupta, M.Z. Vatamaniuk, C.S. Lee, R.C. Flaschen, J.T. Fulmer, F.M. Matschinsky, S.A. Duncan, K.H. Kaestner, The MODY1 gene HNF-4alpha regulates selected genes involved in insulin secretion, J. Clin. Invest. 115 (2005) 1006–1015.

[33] T. Gao, B. McKenna, C. Li, M. Reichert, J. Nguyen, T. Singh, C. Yang, A. Pannikar, N. Doliba, T. Zhang, D.A. Stoffers, H. Edlund, F. Matschinsky, R. Stein, B.Z. Stanger, Pdx1 maintains beta cell identity and function by repressing an alpha cell program, Cell Metab. 19 (2014) 259–271.

[34] M.A. Hale, H. Kagami, L. Shi, A.M. Holland, H.P. Elsasser, R.E. Hammer, R.J. MacDonald, The homeodomain protein PDX1 is required at mid-pancreatic development for the formation of the exocrine pancreas, Dev. Biol. 286 (2005) 225–237.

[35] M. Brissova, M. Shiota, W.E. Nicholson, M. Gannon, S.M. Knobel, D.W. Piston, C.V. Wright, A.C. Powers, Reduction in pancreatic transcription factor PDX-1 impairs glucose-stimulated insulin secretion, J. Biol. Chem. 277 (2002) 11225–11232.

[36] B.R. Gauthier, A. Wiederkehr, M. Baquie, C. Dai, A.C. Powers, J. Kerr-Conte, F. Pattou, R.J. MacDonald, J. Ferrer, C.B. Wollheim, PDX1 deficiency causes mitochondrial dysfunction and defective insulin secretion through TFAM suppression, Cell Metab. 10 (2009) 110–118.

[37] J. Sun, L.Q. Mao, K.S. Polonsky, D.C. Ren, Pancreatic beta-cell death due to Pdx-1 deficiency requires multi-BH domain protein Bax but not Bak, J. Biol. Chem. 291 (2016) 13529–13534.

[38] B. Koletzko, J. Beyer, B. Brands, H. Demmelmair, V. Grote, G. Haile, D. Gruszfeld, P. Rzehak, P. Socha, M. Weber, G. European Childhood Obesity Trial Study, Early influences of nutrition on postnatal growth, Nestle Nutr. Inst. Workshop Ser. 71 (2013) 11–27.

[39] H. Du, Y. Zhao, J. He, Y. Zhang, H. Xi, M. Liu, J. Ma, L. Wu, YTHDF2 destabilizes m(6)A-containing RNA through direct recruitment of the CCR4-NOT deadenylase complex, Nat. Commun. 7 (2016) 12626.

[40] B.S. Zhao, C. He, "Gamete on" for m6A: YTHDF2 exerts essential functions in female fertility, Mol. Cell 67 (2017) 903–905.

[41] X. Wang, B.S. Zhao, I.A. Roundtree, Z. Lu, D. Han, H. Ma, X. Weng, K. Chen, H. Shi, C. He, N(6)-methyladenosine modulates messenger RNA translation efficiency, Cell 161 (2015) 1388–1399.